Preliminary WFC3 UVIS PSF Evaluation

G. F. Hartig and S. Baggett
25 March 2004

ABSTRACT
We have made an initial assessment of the image quality of the WFC3 UVIS channel with its flight detector installed. Point source measurements at four field positions and four wavelengths indicate excellent imaging performance for the UVIS channel, with CEI encircled energy specifications readily achieved.

Introduction

The flight UVIS CCD detector was aligned at Ball Aerospace to its mounting ring, based on previous measurements of the UVIS pathfinder detector at GSFC, and installed in the WFC3 instrument in November 2003. Alignment check measurements, made with the CASTLE telescope simulator, showed residual misalignment of the detector in excess of expected tolerances. Subsequent analyses showed that an error had been made at Ball during computation of the required alignment offsets, and two independent calculations verified the amended Ball methodology. With the source of the alignment error identified and the immediate impact on the program deemed minor, the flight detector remained in non-optimal alignment for a series of verification and preliminary calibration measurements, obtained in the SSDIF at GSFC in ambient environment in Dec 2003 and Jan 2004.

We discuss the measurements of the UVIS PSF at four field positions, through four filters spanning the spectral range. The residual detector misalignment, after focus compensation with the onboard corrector and adjustment for image location offsets, has minimal effect on the PSF quality at the chosen field points near the centers of each of the quadrants of the FOV. The detector tip/tilt offsets will more noticeably affect the image quality at the FOV corners and render the camera more susceptible to focus drift effects (such as HST OTA "breathing"), if left uncorrected. The measurements were made with the CASTLE "J" alignment, which represents its best-known match to that of the OTA with respect to the WFC3 latches. The UVIS corrector was adjusted slightly in tip/tilt, as well as in focus, to optimize the image quality near field center; the resultant corrector mechanism settings are shown in Table 1. Note that this may not be the ultimate best alignment of the corrector, since optimal balance over the field will likely require

slight detuning at field center. The measurements presented here represent a subset of those planned for final verification of the instrument, in its flight condition and in a flight-like environment. That plan includes PSF evaluation at 16 uniformly distributed field points.

Table 1. UVIS Corrector Mechanism Settings

Focus (LDVT)	2285
Inner Cylinder	9569
Outer Cylinder	53428

Procedure

The PSF data were obtained on 12 Dec 2003 with SMS VE02S05 (image rootnames IV0205xx; IDL database entries 1813:1876; quicklook log ID 2003346a). After a false start, during which the CASTLE chopper had inadvertently drifted into the beam, a full set of data, comprising 64 point-source and bias images, was successfully obtained. To maximize efficiency, 200 px square subarrays, approximately centered on the PSFs near the center of each detector quadrant (field point IDs UVJ13, 14, 15, and 16), were used to obtain pairs of images, through each of four filters: F225W, F336W, F606W and F814W. The CASTLE provided narrow-band point source illumination with a 5 um pinhole, D2 lamp, and double monochromator with 13 nm bandpass, for the UV filter observations and lasers at 633 and 810 nm through single-mode fibers for the R and I band filter data. The detector was operated at –74C, the cold limit of the ambient test environment, rather than the nominal –83C; this difference is expected to have negligible effect on the image quality results.

In addition to the subarray images, deep full frame images with the image cores saturated were also obtained to better assess the PSF far wings and search for straylight effects, such as the CCD scatter halo seen at long wavelengths in the STIS and ACS HRC detectors. Because background images, with point source illumination shuttered, were not obtained, and the background illumination from room lights was fairly strong and structured, the images through F606W and F814W are not deemed useful, except as a test run of the procedure to be used in the thermal vacuum measurements to follow. Also obtained were dark images, following highly saturated PSF images, to evaluate image persistence effects in the CCDs. No significant image persistence was discovered; this will be analyzed in a future ISR.

Results

A montage of the images at each field point and wavelength is displayed, with a log stretch over ~6.5 dex, in Figure 1. The diffraction-induced growth of the PSF with wavelength is apparent. Note the ghost images, with strong field dependence, produced by the F225W filter, even in narrow-band illumination well within the filter passband; these are discussed by Brown and Lupie (2004). The images at UVJ14 suffer from a single blocked column; its effect on the measured EE is insignificant.
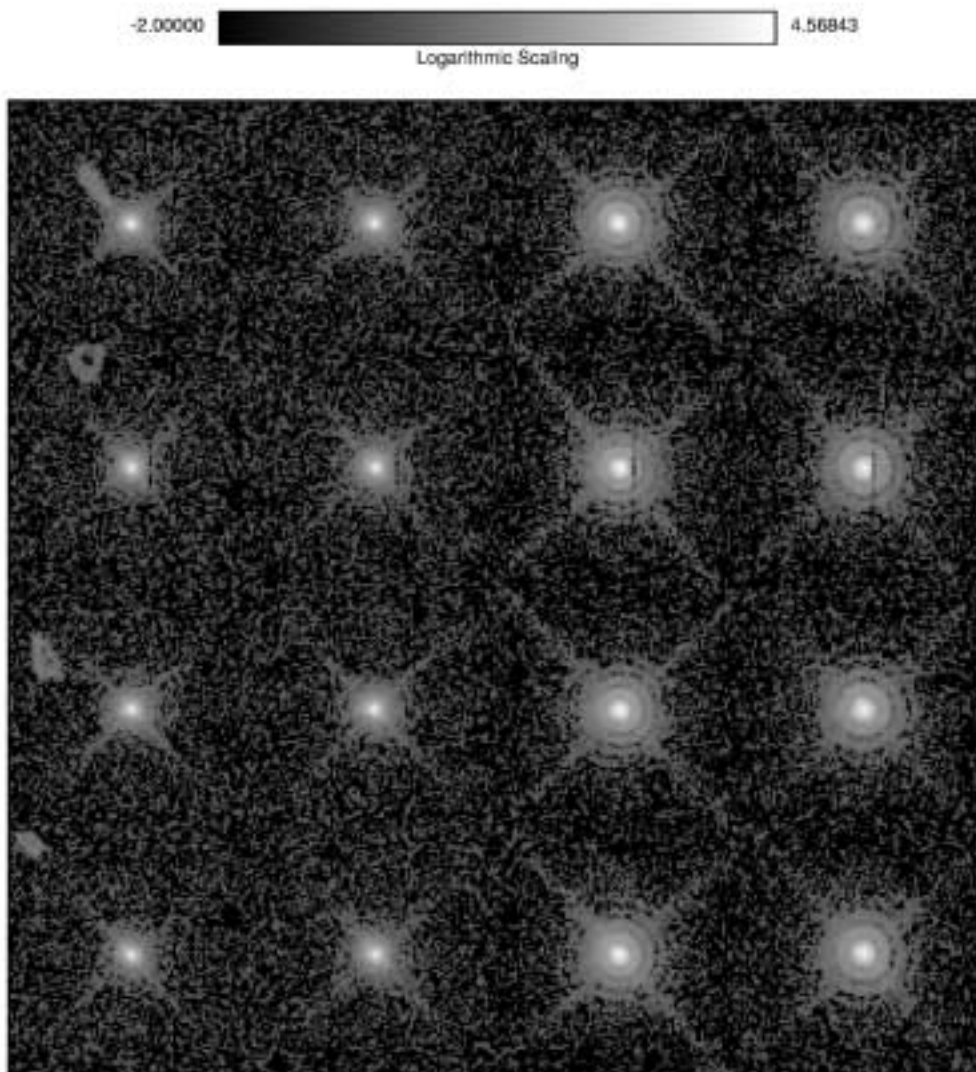
Figure 1. Montage of measured PSF images at field points UVJ13 through UVJ16 (top to bottom) and at wavelengths 250, 350, 633, and 810 nm (left to right). The images have had background subtracted and first-order geometrical distortion removed.

The encircled energy (EE) as function of radius from PSF center was computed for each of the unsaturated images, using IDL code previously developed and used for COSTAR, STIS and ACS alignment and verification. Briefly, the code corrects for first-order geometrical distortion, finds the image center at which the EE in a small diameter (0.15 arcsec) is maximized, computes the radius of each pixel from that center and, after subtracting a background that is adjusted so that the EE curve asymptotes to 1 with 0 gradient at a specified radius (2 arcsec), sums the normalized flux contribution within discrete radii, including estimation of partial pixel contributions. The results are plotted in Figure 2, for each of the measured field points. Also shown are the CEI specification requirement and goals for the EE at 250 and 633 nm; it is apparent that the requirements

are readily achieved and the goals are generally met, at all four field points, *if these EE measurements are taken at face value (see below).*
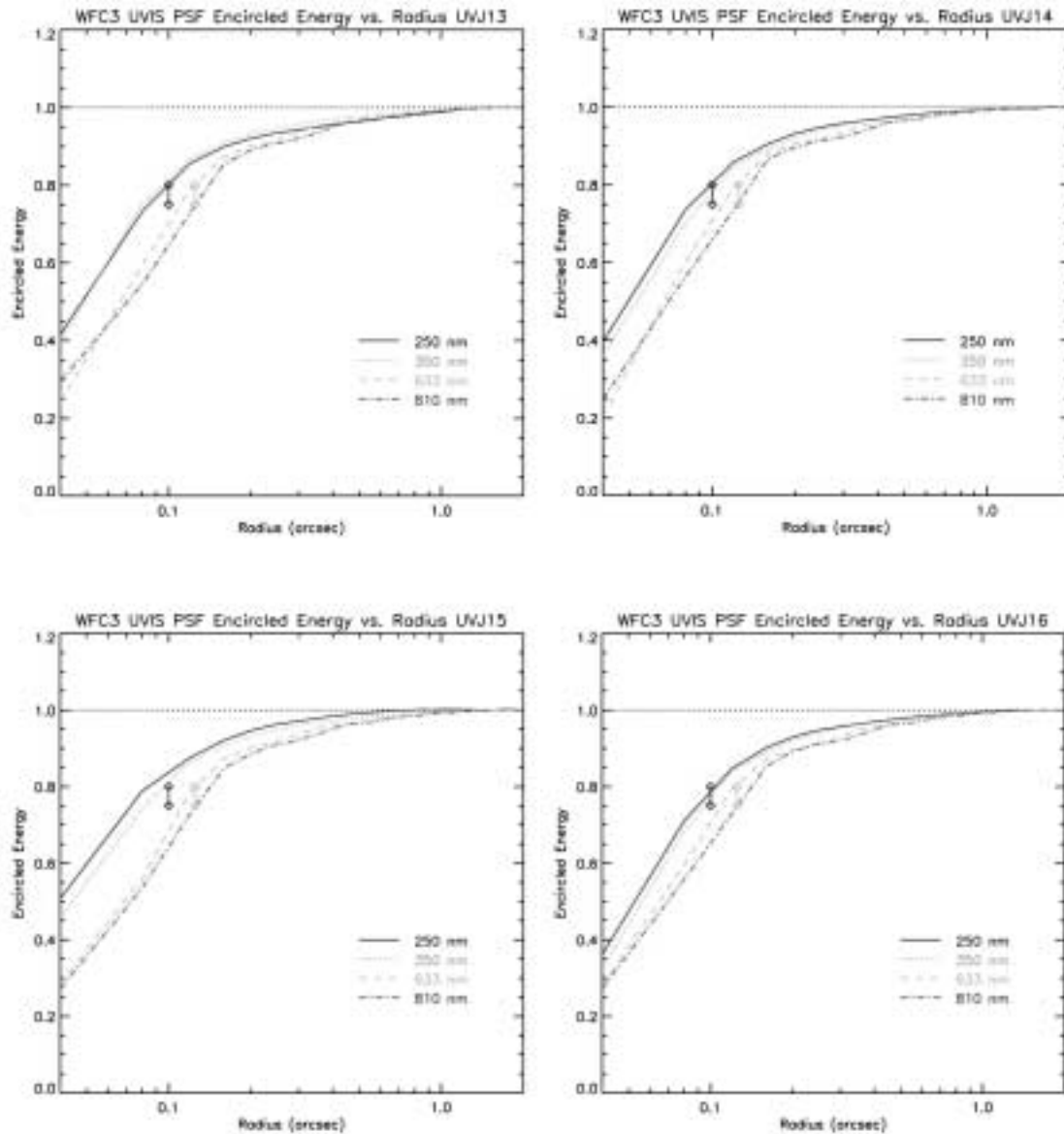
Figure 2. Measured encircled energy as function of radius from image center for 4 field points and 4 wavelengths. The CEI specification requirements and goals are also shown as diamonds for 250 and 633 nm.

The EE within selected radii and the peak pixel fraction (useful for exposure time estimation with regard to saturation avoidance), are presented in Table 2. There are minor differences (~1 %) between the curves in Figure 2 and the Table 2 values; the latter optimize the image center for each diameter, resulting in slightly higher EE in some cases. Note that the peak fraction is highly sensitive to centration on the pixel grid, especially at short wavelengths where the Airy disk is undersampled. Modeling (see

below) shows that PSFs centered on the pixel corners can produce peak fraction 5% (absolute) lower than those centered on a pixel, at 250 nm.

Table 2. Measured Encircled Energy and Peak Fraction

UVJ13					
λ (nm)	Peak	0.15	0.2	0.25	0.35
250	0.170	0.730	0.821	0.866	0.909
350	0.183	0.714	0.821	0.870	0.917
633	0.143	0.573	0.717	0.815	0.888
810	0.129	0.52	0.631	0.747	0.868

UVJ14					
λ (nm)	Peak	0.15	0.2	0.25	0.35
250	0.147	0.711	0.811	0.862	0.916
350	0.154	0.694	0.808	0.859	0.908
633	0.111	0.563	0.709	0.814	0.893
810	0.108	0.523	0.645	0.765	0.879

UVJ15					
λ (nm)	Peak	0.15	0.2	0.25	0.35
250	0.160	0.731	0.832	0.884	0.932
350	0.125	0.689	0.808	0.865	0.915
633	0.129	0.564	0.710	0.809	0.887
810	0.113	0.506	0.623	0.741	0.864

UVJ16					
λ (nm)	Peak	0.15	0.2	0.25	0.35
250	0.173	0.711	0.810	0.860	0.915
350	0.160	0.681	0.796	0.849	0.905
633	0.141	0.556	0.701	0.801	0.882
810	0.110	0.513	0.629	0.748	0.870

We have attempted to assess the validity of our image modeling by comparison with the CASTLE measurements. We simulated the CASTLE image at 633nm using the low-order Zernike coefficients describing the WFE at theUVJ16 field point, as measured by phase retrieval from a through-focus image series obtained during the alignment check shortly before these PSF measurements. About 15 mas of gaussian jitter, in addition to the low-order WFE, was required to effectively match the measured EE curve at 633nm, as shown in Figure 3 (lower curves). This may be reasonably attributed to the CCD MTF. A measurement made at the GSFC Detector Characterization Lab of the pixel response of a similar CCD to a very small spot at 850 nm indicates that 72% of the energy falls within the central pixel (Foltz, 2004). A simulation has shown that this corresponds to the peak energy fraction of a delta function convolved with 14 mas RMS of gaussian jitter, in excellent agreement with our finding. Thus, with the measured EE demonstrating a good match, at radii from 0.04 (1 px) to 2 arcsec, to a model including only an independent

assessment of the low order WFE, the pupil mask and a reasonable estimate of the detector MTF, we may be confident in our image quality assessments.
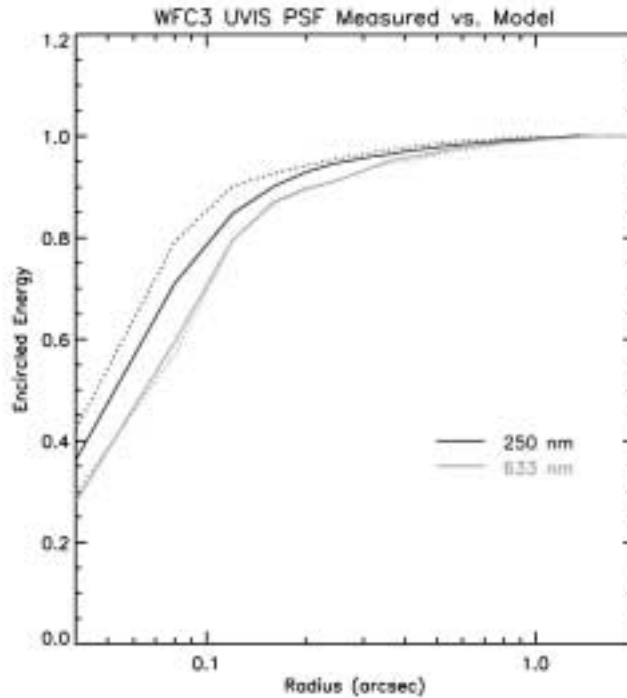
Figure 3. Comparison of measured (solid) and model (dotted) PSF EE curves at 250 and 633 nm. The departure from the model at 250 nm is attributed to CCD charge diffusion.

The same model computation was performed at 250 nm and compared to the measured EE (Figure 3, upper curves). The model over-predicts the EE, especially at radii <0.2 arcsec. This is expected, since backside-illuminated CCDs demonstrate MTF degradation at short wavelengths, due to diffusion of signal electrons, created very near to the illuminated surface of the CCD where the pixel-defining potential wells are ineffective, into neighboring pixels. Increasing the model jitter from 15 to 25 mas (or ~60% of the px width) produces a reasonable match to the EE curve at 250 nm. A similar effect was seen in the ACS HRC, where 60% px width RMS jitter was also used in the modeling. Table 3 presents the inferred pixel response function kernels, with which model PSFs are to be convolved, at 250 and 850 nm. Note that the CEI specification for PRF (sec 4.6.3) requires that 90% of the energy from a 5 μ centered spot lie within a pixel; this is clearly not met at any wavelength.

Table 3. CCD Pixel Response Functions

250 nm			850 nm		
0.04	0.12	0.04	0.006	0.064	0.006
0.12	0.35	0.12	0.064	0.720	0.064
0.04	0.12	0.04	0.006	0.064	0.006

The EE specification applies to the WFC3 installed in the HST, and differences between the CASTLE and HST must be accounted for to predict on-orbit performance. We have modeled PSFs for both the HST OTA and for CASTLE, which has wider spiders and a larger (0.46 vs. 0.33) central obscuration, redistributing energy from the Airy disk into (predominantly) the first ring. These differences affect the EE in the specified diameters (0.2 and 0.25 arcsec) significantly, producing about 5% higher EE (at the specified diameter, for either 250 or 633 nm) with the more favorable OTA pupil. The low-spatial frequency wavefront error (WFE) match of CASTLE to the HST OTA is very close, by design, and should not result in substantive differences in the EE (Greeley, et al. 2003). We have no direct way of assessing the degree to which the CASTLE images may be affected by jitter or atmospheric effects, although exposure times were typically short (1-20 s), so image degradation due to slow drift should be negligible. Nor do we have direct measurement of CASTLE mid-spatial frequency WFE, but it cannot strongly affect the PSF, given the good agreement with our model.

However, the OTA mid-frequency WFE is significant and fairly well known, having been mapped on-orbit with phase retrieval analysis of a series of WFPC2 images at various defocus settings of the secondary mirror (Krist and Burrows, 1995). These mirror maps have been previously used to produce model images that are a good match to the measured on-orbit performance of the ACS (Hartig, et al., 2002), over the spectral range of interest. Modeling of the WFC3 UVIS and HST shows that inclusion of the mirror map WFE has a substantial effect, moving significant energy from the core into the wings of the PSF, especially in the UV. The EE in 0.2 arcsec at 250nm will degrade by ~15%, while the EE in 0.25 arcsec at 633 nm drops ~3%, when these mid-frequency errors are added to the nominal OTA+UVIS image simulation. Thus, adjusting the values measured with CASTLE to include the OTA pupil and mid-frequency WFE, our current best estimate of the EE achieved on orbit is ~72% in 0.2 arcsec at 250 nm, and 83% in 0.25 arcsec at 633 nm. While the latter exceeds the specified goal, the former falls below the requirement (75%), which was ill-conceived, given the known OTA performance, and is not indicative of lack of performance of the WFC3 UVIS channel.

The images analyzed above were obtained with single exposures, with typically about 30 ke$^-$ in the peak pixel. To construct a much deeper image in order to better evaluate the PSF wings, we also obtained saturated images, with the peak pixel ~5 and 50 times the full well level. The saturated pixels and their immediate neighbors were replaced with scaled versions of the shorter exposures, thereby creating a low-noise, high dynamic range image. The combined image obtained at field point UVJ14 at 350 nm, with about 2.2 Me$^-$ in the peak pixel is shown on a log stretch, cropped to ~16 arcsec square, in Figure 4. There are several spurious features readily apparent in the image, including a streak at position angle (PA) ~265 deg (caused by a grazing incidence reflection on a baffle above the CASTLE source plane), two "blobs" near the spider diffraction spikes at PA 134 and 314 (source indeterminate), a couple of cosmic ray hits, a partially blocked column (2868), and some donut-shaped optical ghosts due to reflections from the various surfaces of the two detector windows. The pairs of "blobs" are interesting; they are apparently a diffraction phenomenon, since their symmetrical distance from PSF center is proportional to wavelength, and they must arise after the flat steering mirrors in

CASTLE, since their PA does not change with field position (as does that of the spider diffraction, due to the pupil-rotating effect of tilting the CASTLE flats). Since the effect is seen at multiple field points, it is likely that it arises near a pupil, such as the UVIS M2 mirror.
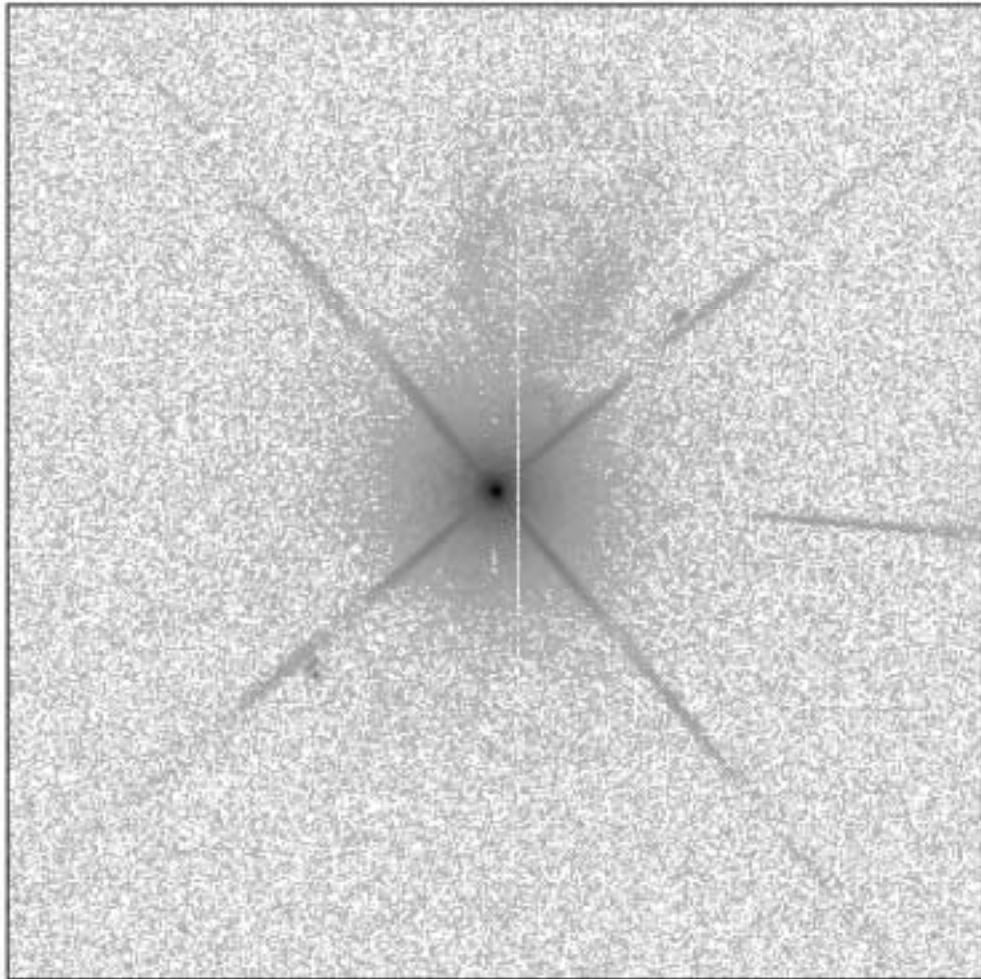
Figure 4. High dynamic range composite PSF at 350 nm at field point UVJ14

After making very minor corrections in the composite image for the CR hits, the blocked column, and the CASTLE "streak", we have computed the EE and azimuthally-averaged (AA) PSF, normalized to 1 at the peak, for comparison with model and specifications. These are shown in Figure 5, which plots the measured EE (left panel) and AA PSF intensity (right panel) as solid lines, with the CASTLE+WFC3 model shown as dotted lines. The agreement between measurement and model is excellent, from radii of 40 mas (1px) to 5 arcsec. The differences in modulation of the AA PSF wings beyond 1 arcsec are at least partially due to inaccuracies in the model related to the diffraction of the spiders. The EE specifications in the PSF wings (actually for 250 nm) are shown as diamonds; again, if taken at face value, the plot indicates that the camera readily meets its requirements. Actual on-orbit performance at 350 nm, including the HST telescope

properties, is approximated by the dashed OTA+WFC3 model curves, which show the effects on the near wings of the mid-frequency WFE.
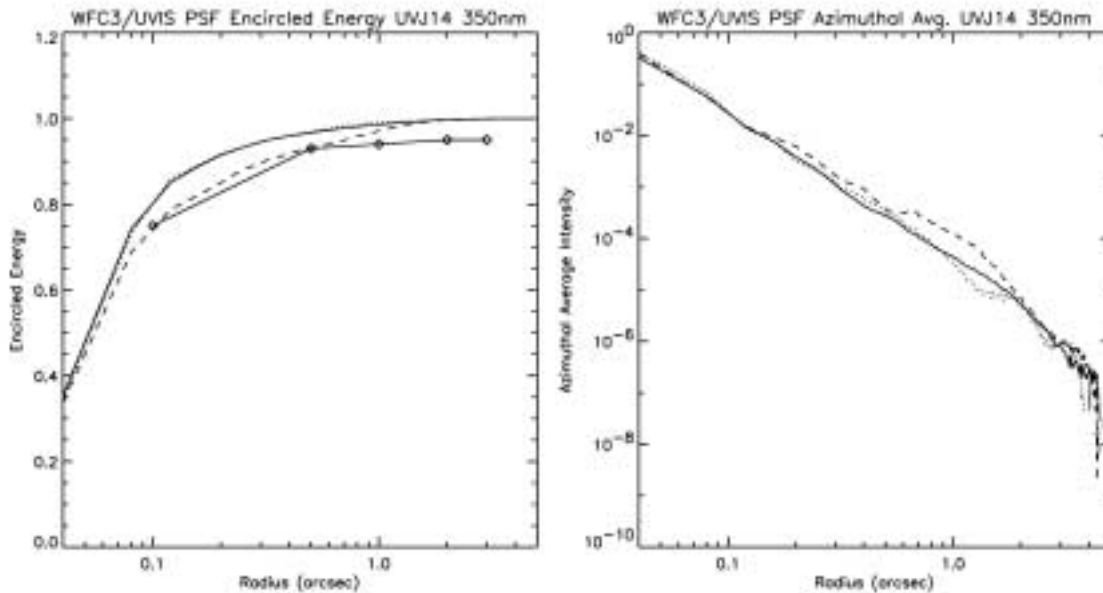
Figure 5. Comparison of composite measured (solid line), CASTLE model (dotted line), and OTA model (dashed line) images at field point UVJ14 at 350 nm. The left frame shows the encircled energy, from radii of 1 px to 5 arcsec, and the right frame plots the azimuthally-averaged PSF. The EE specifications (at 250 nm) are shown as diamonds.

Conclusion

On the basis of our analysis of this initial, incomplete look at the image quality of the WFC3 UVIS channel, we conclude that the instrument optical performance is generally excellent. Aside from the anomalous filter ghosts, such as those readily apparent in the F225W images (see Brown, et al 2004, for a complete discussion) and a symmetrical pair of weak straylight features whose genesis is not yet understood, the UVIS channel is performing as expected at the four field points examined here. One caveat to this conclusion is that the measurements were made in the ambient environment of the SSDIF, with the optical bench running warmer than room temperature, while it will be at ~ 0 C in orbit; any optical misalignment that is not correctable with the corrector mechanism (focus and pupil alignment) may result in a degradation of optical performance. A more comprehensive evaluation, with deeper images at 16 field points, will occur during the thermal vacuum testing planned for summer 2004, in which the optical bench will operate near its expected on-orbit temperature.

Our modeling indicates that the UVIS channel will readily meet its on-orbit image quality (EE) specifications at 633 nm, but that the requirements at 250 nm will not be achievable, through no fault of the WFC3, due to the mid-frequency WFE of the HST OTA. A waiver or amendment of the 250 nm EE requirements is in order. The CCD pixel response function specification will also not be met at any wavelength.

References

Brown, T. and Lupie, O. "Filter Ghosts in the WFC3 UVIS Channel", STScI ISR WFC3-2004-04, 2004.

Foltz, R. "Single Pixel Illumination Report", GSFC DCL Internal Report, 2004.

Greeley, B., et al. "CASTLE Acceptance Test Report, WFC3-BWG-577-011- DRAFT", 20 Feb 2003.

Hartig, G.F, et al. "On-orbit Alignment and Imaging Performance of the HST Advanced Camera for Surveys", Proc. S.P.I.E. **4854**, 532, 2002.

Krist, J.E. and Burrows, C.J. "Phase Retrieval Analysis of Pre- and Post-Repair Hubble Space Telescope Images", Applied Optics, **34**, 4951, 1995.